INTERNATIONAL JOURNAL OF HYDROGEN ENERGY 40 (2015) 8889–8896

Available online at www.sciencedirect.com

ScienceDirect

journal homepage: www.elsevier.com/locate/he

Electrochemical performance of lithium molybdenum composite catalyst in oxygen reduction reaction

A. Ongun Yüce [a], M. Farsak [b], F.S. Akgül [a], F. Tezcan [a], E. Telli [c], G. Kardaş [a,*]

[a] Çukurova University, Faculty of Letters and Science, Department of Chemistry, 01330 Balcalı, Adana, Turkey
[b] Osmaniye Korkut Ata University, Faculty of Letters and Science, Department of Chemistry, 80000 Karacaoğlan Campus, Osmaniye, Turkey
[c] Osmaniye Korkut Ata University, Faculty of Engineering, Department of Engineering Systems, 80000 Karacaoğlan Campus, Osmaniye, Turkey

ARTICLE INFO

Article history:
Received 1 April 2015
Received in revised form
7 May 2015
Accepted 8 May 2015
Available online 4 June 2015

Keywords:
Oxygen reduction reaction
Catalyst
Lithium
Molybdenum
TEM

ABSTRACT

A gel/LiMo catalyst was prepared as a cathode material via the sol–gel process and applied calcination at different times. The influence of calcination times, properties and the electrochemical performance of the catalyst were investigated by utilizing cyclic voltammetry, potentiodynamic polarization and electrochemical impedance spectroscopy techniques. The surface of the catalysts, which were prepared in different combinations were physically characterized using X-ray diffraction, scanning electron microscopy (SEM) and transmission electron microscopy (TEM). The SEM and TEM images showed that among the different catalysts, the gel@LiMo catalyst has a different crystal structure. The gel/LiMo catalyst shows good electrochemical performances in an organic solution and has a good structural stability. The catalysts also illustrated great electrochemical performances in the oxygen reduction and evolution reactions.

Introduction

During the last two decades, lithium air batteries have been the subject of intense study because of their high energy capacity in electric and hybrid vehicles [1–3]. Lithium air battery is to be known as one of the most attractive metal-air battery systems due to its the highest energy density per weight unit. In lithium air batteries, the discharge reaction occurs between lithium and oxygen yielding Li_2O or Li_2O_2, and the theoretical specific energy density of this reaction is 5200 Wh kg^{-1}. Practically, the storage of oxygen is not required, since air can be used directly in the battery. Therefore, the theoretical specific energy density (excluding oxygen) is 11,140 Wh kg^{-1} [4] which is higher than Li-ion batteries [5] and other developed batteries [6,7]. Generally, lithium air batteries with a high energy density contain a lithium anode, an air cathode supplying the oxygen and a non aqueous electrolyte. During

* *Corresponding author*. Tel.: +90 322 338 6081x2593; fax: +90 322 338 6070.
E-mail addresses: gulfeza@cu.edu.tr, gulfeza@gmail.com (G. Kardaş).
http://dx.doi.org/10.1016/j.ijhydene.2015.05.050

discharge in lithium air batteries, the following reactions take place at both the anode and the cathode:

Cathode (discharge reaction):

$$2Li^+ + 2e^- + O_2 \rightarrow Li_2O_2 \quad (1)$$

$$4Li^+ + 4e^- + O_2 \rightarrow 2Li_2O \quad (2)$$

Anode (discharge reaction):

$$Li \rightarrow Li^+ + e^- \quad (3)$$

The reversible cathode reaction occurs in lithium air batteries but the disadvantages of this process is that these reactions are slow. Hence, charge and discharge reactions in lithium air batteries should be enhanced by using effective catalysts.

The air cathode preparation method can be performed by the different strategies, such as rolling, spreading, casting, coating and spray. Several novel methods have also been developed, in recent years, to enhance the battery performance [8]. The air cathode was made with a new method by S. D. Beattie et al., they prepared the slurry of NMP/PVdF/carbon mixture and rolled onto the nickel foam by sonicated and then removed the NMP by heating [9]. Yanming et al. improved a free-standing-type air electrode by a chemical deposition reaction, they deposited Co_3O_4 on the nickel foam without binder and carbon matrix [10]. Petru et al. reported that partly wetted air cathodes, which have nonuniform distribution, can develope the capacity of lithium-air batteries [11]. Crowther et al. [12] and Zhang et al. [13] suggested approaches named as mineral spirits and filtration, respectively [6]. Some good results are increasingly being obtained with the application of advanced materials and new methods [14].

Platinum nanoparticles shows a unique catalytic properties because of high electronic conductivity and stability [15]. In addition; platinum composites with low cost metal and their oxides such as vanadium, molybdenum, cobalt, chromium, and iron oxides also exhibit good catalytic efficiency towards ORR along [16,17].

The researches were focused on to improve the multicomponent materials using nonprecious metals for the more active, stable and cheaper electrocatalysts. Many transitional metal oxides, MnO_2 [18], Fe_2O_3 [19] Pd/MnO_2 [20,21] and Pt–Au nanoparticle [22] have been reported as effective catalysts for this purpose. However, formation of lithium oxides and peroxides during the discharge reactions affect the cathode negatively. To prevent the negative effect, lithium-air batteries need good cathode materials. According to literatures, there are several criteria for the good cathode material, one of them is the crystal structure [23] and the another one the particle size. Studies reveals that the optimum particle size for a cathode material may vary depending on the type of composite used such as lithium transition metal oxides in which Li^+ ions diffuse more rapidly in nanometer size particles [24] than in large particles [25]. Also, the calcination temperature has an effect on the preferred particle size [26,27]. Transition metals and their oxides are skilled to form chemical bonds with O_2 using their d orbitals [16], because of this properties, they have also been investigated as nonprecious metal electrocatalysts for ORR [28,29]. Recently studies, molybdenum oxides are highly popular because of their unique electronic and molecular structures in many catalytic applications [30]. This can be attributed to the non-stoichiometric lower valence compositions between MoO_2 and MoO_3 simply given as MoOx [16,31].

The purpose of this study is to prepare lithium molybdenum bifunctional catalysts, calcined at 500 °C at different calcination times for MoO_3. That is why, gel, $LiNO_3$ and MoO_3 were used to set a matrix for bifunctional structure and to enhance the oxygen reduction (ORR) and evolution reactions (OER), respectively. When lithium ions move into the spinal matrix, the electrocatalytic activity rises toward the enhancing of the OER [32]. The appropriate calcination time for MoO_3 was determined and the prepared catalysts were characterized by using SEM, XRD, TEM and cyclic voltammetry techniques.

Experimental

Gel preparation

The gel/Li and gel/LiMo catalysts were prepared by the sol–gel process: $LiNO_3$ (Alfa Aesar, 99%) and MoO_3 (Merck for analysis) were used as metal ion sources (in the mole ratio of Li:Mo (1:1,5)), glycine ($C_2O_2NH_5$, Merck, 98.5%) as a chelating agent and glycerol (Panreac, M = 92,10) as a dispersant agent. Activated carbon was used to enhance the electrical conductivity. Glycine, glycerol, ammonia, lithium and MoO_3, which was calcinated during 8 h before the catalyst preparation, were mixed in a pressure resistant Schlenk tube. Then 120 °C was applied during 12 h to obtain a viscous mixture. After that the viscous mixture was statically aging for 24 h at room temperature. Following this process, one part of the gel was rolled and left to paste on a stainless steel plate (SS) at 170 °C for 8 h in order to make an electrode. This catalyst preparation method has been illustrated in our previous paper [32].

Preparation of catalysts

The working electrode was a circular disc cut from a stainless steel (SS) rod using stainless steel cutting machine. The metal disc was coated with polyester except its bottom surface with the surface area of 0.126 cm^2. The prepared gels were rolled up on SS and kept on hold in an oven at 125 °C for 4 days. In this study, the gels prepared in the absence of MoO_3 were called gel/Li and the gels prepared with uncalcined and calcined MoO_3 at 500 °C at different calcination times (5, 8, 15 h) were called gel/LiMo and gel@LiMo, respectively.

Electrolyte

The electrochemical analyzes were performed in lithium perchlorate (10%), ethylene carbonate (45%) and dimethyl carbonate (45%) (LED) solution. The electrolytes were prepared from analytical grade chemical reagents and used without

further purification. Freshly prepared solutions were used for each analysis. During the experiments, the test solutions were opened to the air, and the experiments were performed under static conditions. The temperatures of solutions were kept at 25 °C (within ±1 °C) by controlling the cell temperature.

Electrochemical measurements

Gamry (interface 1000) model electrochemical analyzer (serial number: 02009) was used for electrochemical measurements under computer control. All electrochemical experiments were carried out with the three electrode technique. The auxiliary electrode was a platinum sheet with a surface area of 2 cm^2. The quasireference electrode (QRE) such as Ag and Pt which doesn't contaminate the test solution with undesirable species is often employed for non aqueous solvents. Therefore, the platinum wire (with 1.188 V vs. SHE) was used as the reference electrode. All potential data given in this study refers to this electrode. The polarization curves were obtained potentiodynamically between the potential ranges from open circuit potential to −3.0 V with the scan rate of 0.10 V s^{-1}. The electrochemical impedance spectroscopy experiments were conducted in the frequency range of 100 kHz–0.003 Hz at open circuit potential by applying alternating current signal of 0.005 V peak-to-peak.

The cyclic voltammetry experiments were conducted at the scan rate of 100 mV s^{-1} between −3.0 V and 1.5 V using Gamry (interface 1000) model electrochemical analyzer. The crystalline phases of gel/LiMo and gel@LiMo catalysts were identified by X-ray diffraction (XRD, Rigaku, Rint-2000) using Cu K_ line at the scanning rate of 4° min^{-1} from 10° to 90°. The surface morphology of gel/LiMo and gel@LiMo catalysts were observed by scanning electron microscopy (SEM). Nitrogen adsorption–desorption measurements for gel/LiMo and gel@LiMo catalysts were carried out using Gemini VII 2390 analyzer at 77 K. Also, surface area, pore size and pore volume for these catalysts was computed using experimental points at a relative pressure of P/P_0 = 0.4–1.0 by the Brunauer–Emmett–Teller (BET) method. TEM observation was obtained using a JEOL JEM 2100F HRTEM 80 kV–200 kV (in five stages: 80.0 kV, 100.0 kV, 120.0 kV, 160.0 kV and 200.0 kV). As for the oxygen evolution reaction (OER) and the oxygen reduction reaction (ORR), the curves were carried out using lithium metal, gel@LiMo and Whatman GF/D as the anode, cathode and separator, respectively with Swagelok type test cell (MTI corporation).

Results and discussion

Electrochemical measurements

Cyclic voltammetry

The cyclic voltammograms of electrodes, prepared of gel, gel+$LiNO_3$ (gel/Li), gel+$LiNO_3$+MoO_3 (gel/LiMo) and activated carbon supported gel+$LiNO_3$+MoO_3 (gel/LiMo-C) obtained in LED solution are shown in Fig. 1. Addition of metal in the gel increased the oxygen reduction reaction and catalytic efficiency. When the metal salts and metal oxides are added in the cathode material, the electrocatalytic efficiency of the lithium air battery can be improved [9]. Metals added catalysts shown higher current density than including only gel electrodes. When the metals added catalyst supported with carbon, which is called as gel/LiMo-C, The highest current density was observed. By adding carbon in the cathode material, electrical conductivity, porosity and performance are enhanced [33]. The current density rises due to the widening of peaks and the lineage of peak potentials to positive and negative directions in the anodic and cathodic area, respectively.

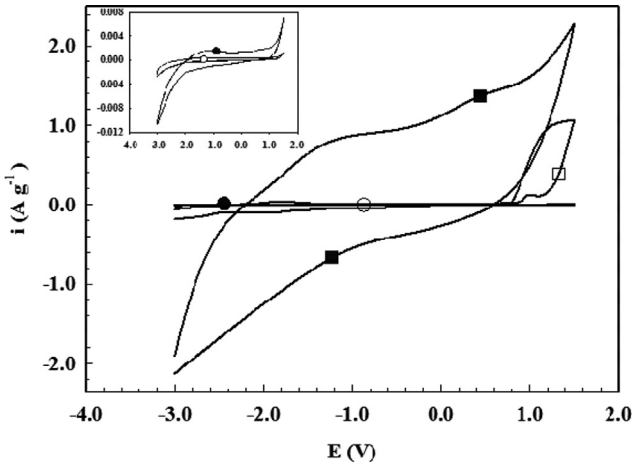

Fig. 1 – Cyclic voltammograms of gel (○), gel/Li (●), gel/LiMo(□) and gel/LiMo-C (■) electrodes at 100 mV s^{-1} scan rate in LED solution.

Cyclic voltammograms obtained for gel/LiMo-C and gel@/LiMo catalysts at different times at 500 °C in an oxygenated environment in LED solution are seen in Fig. 2. When voltammograms of catalysts are examined, it is shown from Fig. 2 that the gel/LiMo-C (prepared with non-calcined MoO_3) catalyst has the lowest current densities. The current density values in the anodic direction with the gel@LiMo catalysts for 15 h and 8 h are close to each other and the highest density

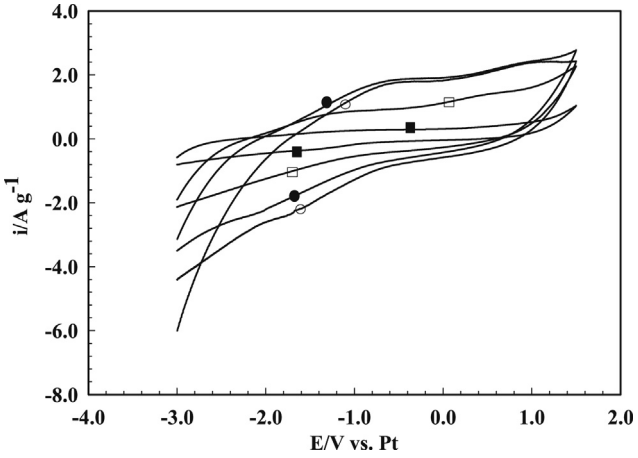

Fig. 2 – Cylic voltamograms obtained from gel/LiMo-C catalysts (■) and calcined gel@LiMo at different times (5 h (▫), 8 h (○), 15 h (●)) at 500 °C in an oxygenated environment in LED solution.

can be found with the gel@LiMo catalyst in 8 h in the cathodic direction. It has been reported that MoO_3 hexagonal structure (h-MoO_3) converts to α-MoO_3 (orthorhombic) structure which is more stable at a temperature above 450 °C [34].

After this section, we used gel@LiMo catalyst, which was prepared with 8 h calcinated MoO_3.

Cathodic polarization curves

The cathodic polarization curves obtained from SS electrode, gel/Li and gel@LiMoO_3, which was prepared with 8 h calcinated MoO_3, catalysts in oxygenated LED solution are shown in Fig. 3. The increase in current density observed from the open circuit potential to −3.00 V in cathodic polarization curves for each electrode is related to the reduction of oxygen to superoxide anion and the formation of Li_xO_x species. The current density is affected by adding metal oxide to the gel in order to activate the catalyst surface [35]. From the catalytic point of view, the gel@LiMo catalyst showed higher catalytic activity than the other gel/Li catalyst. The lowest current density is seen at the SS electrode. The open circuit potentials of the SS electrode, gel/Li and gel@LiMo catalysts in the same environment were obtained as −0.185 V, −0.146 V and −0.104 V, respectively. The open circuit potential of the gel@LiMo catalyst shifted to more positive potentials compared to the gel/Li catalyst. The formation of superoxide anion and the conversion to Li_xO_x species are realized in the gel@LiMo catalyst in lower potentials than the gel/Li catalyst. This comes from the gel@LiMo catalysts have a higher catalytic activity than the gel/Li and the SS electrode.

EIS measurements

Fig. 4 shows the Nyquist, Bode and the phase angle-frequency curves obtained at the open circuit potential of SS electrode, gel/Li and gel@LiMo catalysts in an oxygenated environment in LED solution. As seen in Fig. 4a, the Nyquist plots exhibited a capacitive loop in the high frequency region and a straight line in low frequencies for catalysts. The capacitive loop in the high frequency is related with charge transfer resistance (R_{ct}) and diffuse layer resistance (R_d) while the straight line in low frequencies corresponds to the diffusion process and represents the Warburg impedance, which is related to the solid-state diffusion of Li^+ in the electrode [36,37]. In the evaluation of Nyquist plots according to the theory, the difference in real impedance at lower and higher frequencies is commonly considered as a charge transfer resistance. The charge transfer resistance must be corresponding to the resistance of the

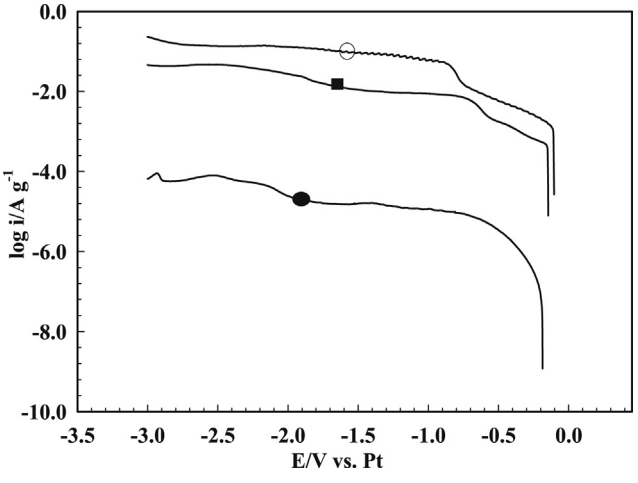

Fig. 3 – Current-potential curves obtained from gel/Li (■) and gel@LiMo (○) catalysts and SS (●) electrode in oxygenated LED solution.

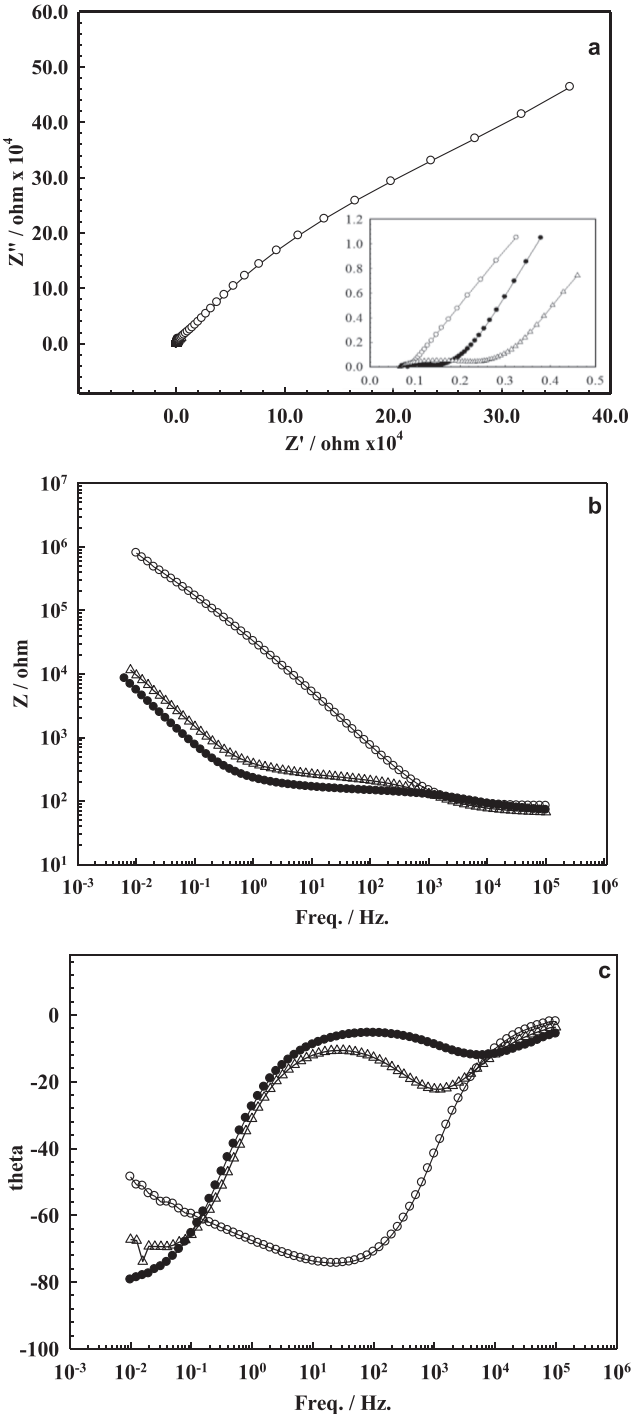

Fig. 4 – Nyquist (a), Bode, (b) and the phase angle-frequency (c) curves obtained at the open circuit potential of SS electrode (○), gel/Li (●), gel@LiMo (△) catalysts in an oxygenated environment in LED solution.

metal-OHP (outer Helmholtz plane) interface. The contributions of all resistances correspond to the metal/solution interface. That is why charge transfer resistance (R_{ct}), diffuse layer resistance (R_d), accumulation resistance (R_a), film resistance (R_f), etc., must be taken into account. The difference in real impedance at lower and higher frequencies is considered as the polarization resistance (R_p) [38,39]. However, in this study, the polarization resistance (R_p) was calculated from Bode plots due to the straight line in low frequencies.

R_p values obtained from Bode plots for SS electrode, gel/Li and gel@LiMo catalysts in Fig. 4 (b) were found as 789.0 kΩ, 11.7 Ω and 6.6 kΩ, respectively. The lowest R_p was obtained with the gel@LiMo catalyst which has the lowest slope in Bode plots. The decrease of R_p values may be associated with the rapid electron transfer in the metal-solution interface towards the working environment. An increase in the catalytic activity of the electrodes and the electrochemical reactions occurring at the interface are easier in the gel@LiMo catalyst. Also, this condition represents the decrease in the polarization resistance as a result of the acceleration of the charge transfer kinetics, falling in the charge transfer resistance (R_{ct}). At the same time, the decrease of a single loop observed in high-frequency in the gel@LiMo catalyst can be explained by the deviation from the semicircle given in EIS theory, frequency scattering and surface roughness. The phase angle-frequency plots are supported by the Nyquist and Bode plots. As to the phase angle curves, for SS electrodes a plot outgoing to 45° is observed. This shows that the charge transfer resistance is quite high in the SS electrode. Apposed to that, the gel/Li and gel@LiMo catalysts are illustrated with closed single loops in the phase angle plots. The lowest phase angle is shown with the gel@LiMo catalyst. This also shows that, the charge transfer resistance of gel@LiMo is lower than the gel/Li catalyst.

Further, the EIS data and to arrange them equivalent circuit models, shown in Fig. 5, were used. The fitting parameters are listed in Table 1 in Fig. 9: R_s is the solution resistance between the working and reference electrodes, R_1 is the charge transfer resistance (R_{ct}), R_2 is the pore resistance (R_{por}) pointing the rough regions and pores, W is Warburg impedance. CPE_1, CPE_2 and Z_w represent the capacitance of the surface layer, the capacitance of the double-layer and Warburg impedance, respectively [40–42]. As it is seen in Table 1, as R_p values decreased in order of SS, gel/Li, gel@LiMo catalysts, and *CPE* values increased in the same order. The CPE_2 value related to porosity of the gel@LiMo catalyst was higher than that of the SS and gel/Li catalysts. These results illustrated that adding MoO_3 to the gel/Li further increased the ORR activity and porosity in the electroactive sites of the surface. The phase shift "n", explained as the degree of surface inhomogeneity, was lower than 1.0, which indicates that the gel@LiMo catalyst had a porous structure.

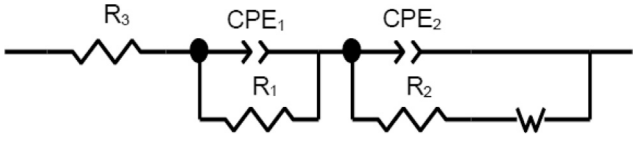

Fig. 5 – Equivalent electrical circuit for gel/Li (●) and gel@LiMo (△) catalysts and SS(o) electrode used to fit the experimental data.

Characterization of catalyst

SEM images of the SS electrode, gel/Li and gel@LiMo catalysts are shown in Fig. 6. In Fig. 6a, only sanding marks are seen on the surface of SS. A glance at Fig. 6b reveals that the gel/Li catalyst which contains structures with stacked small particles (after 125 °C and 4 days) is porous. Referring to Fig 6c, it is observed that the surface morphology of the gel/Li catalyst changes with the addition of MoO_3 into the gel/Li matrix. The gel@LiMo catalyst has a honeycomb-like surface which is brighter and more porous 8 h after calcination. This particular morphology is evaluated as the most favorable one in terms of the catalyst performance since it has a high electrocatalytic activity. The SEM results are consistent with the XRD measurements data.

It is known that the calcination time greatly affects crystallinity, structural and electrochemical properties of the active ingredient. As a result of this, it is crucial to choose a suitable calcination time. The XRD pattern of the gel/LiMo and gel@LiMo samples at different times are displayed in Fig. 7. In Fig. 7a and b, the peak intensity which is associated with the hexagonal structure of MoO_3 (h-MoO_3) is observed in the range of 20–30° at 2θ angle (JCPDS – 21-0569). When the calcination time increases, the peak intensity gets smaller which means that longer calcination time could change the crystallinity of MoO_3 found in samples. It is observed that the peak intensity of h-MoO_3 structure decreased at the end of 8 h calcination time (Fig 7c). In the literature, the decrease in peak intensity has been connected to a phase transformation from hexagonal phase to more stable orthorhombic MoO_3 (α-MoO_3) phase as a result of increasing calcination time [34,43]. The increase observed in peak intensity at 15 h (Fig 7d) may be due to a distortion in the crystal structure of α-MoO_3.

Nitrogen adsorption isotherms of gel@LiMo catalysts at 77 K are shown in Fig. 8. The data shows that the gel@LiMo catalyst corresponds to type-III isotherms which indicates presence of macropores and weak adsorption [44]. The pore-size distributions of the gel@LiMo catalyst were determined on the basis of the desorption isotherms by the BET method. The BET surface area, the total pore volume and the pore size for the gel@LiMo catalyst were 68,5792 m^2/g, 0.2017 cm^3/g and ~6 nm respectively. As is known, the cathode material with macropores may facilitate the oxygen diffusion at the non-aqueous electrolyte due to the large active surface area [45]. TEM images of the gel@LiMo samples are given in Fig. 9. The black dots seen stacked on top of each evince that h-MoO_3 returns to the α-MoO_3 (orthorhombic) form [34].

As seen in Fig. 10, OER and ORR curves of the gel@LiMo catalyst were determined at a current density of 0.05 mA cm^{-2}. The voltage gap between oxygen reduction and evolution reactions are occurred due to overpotential in the battery system. The overpotential occurred because the cathode pores had been clogged by Li_xO_x species at discharge process. Had the overpotential been lower the charge and discharge curves would have been close to each other. As seen in the figure, the voltage gap is 0.57 V. In literature, Yang et al. investigated the voltage gap of 50%Pt/C and SCCO-Cu

Table 1 – EIS parameters for the SS electrode, the gel/Li and gel@LiMo catalysts.

	R_1 $\Omega\ cm^2$	CPE_1 $Y_0(\times 10^6 \cdot s^n \cdot \Omega^{-1})$	n_1	R_2 $\Omega\ cm^2$	CPE_2 $Y_0(\times 10^6 \cdot s^n \cdot \Omega^{-1})$	n_2	W
SS	6236	23.86	0.811	611×10^3	17.27	0.907	7.984×10^{-6}
gel/Li	138.5	691.9	0.325	16×10^3	578.2	0.853	29.47×10^{-6}
gel@LiMo	151.9	693.1	0.302	1091	2217	0.847	139.2×10^{-6}

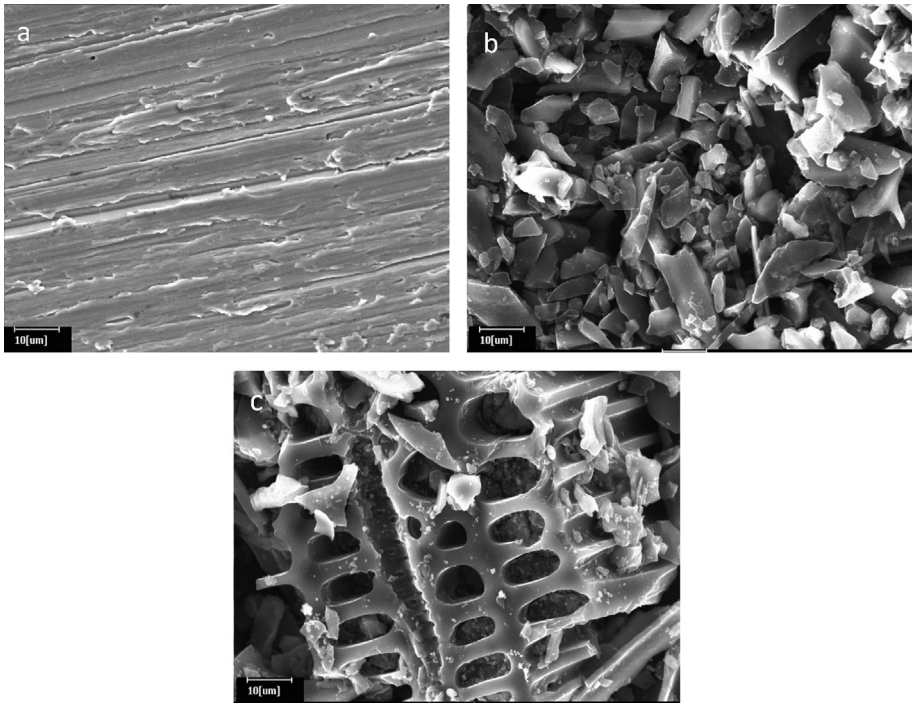

Fig. 6 – SEM images of SS (a), gel/Li (b), gel@LiMo (c).

catalysts, they found 0.68 and 0.98 V, respectively [46,47]. Our another study, we researched gel@LiCu catalyst voltage gap and we found that 0.63 V [32]. Li–Mo bifunctional catalyst improved the oxygen reduction and evolution reactions. For non-aqueous lithium–oxygen battery, LiO_2 and Li_2O_2 are the intermediate and main discharge product with a stable electrolyte, and during discharge/charge processes, the suitable oxygen reduction/evolution reactions (ORR/OER) can be explained as:

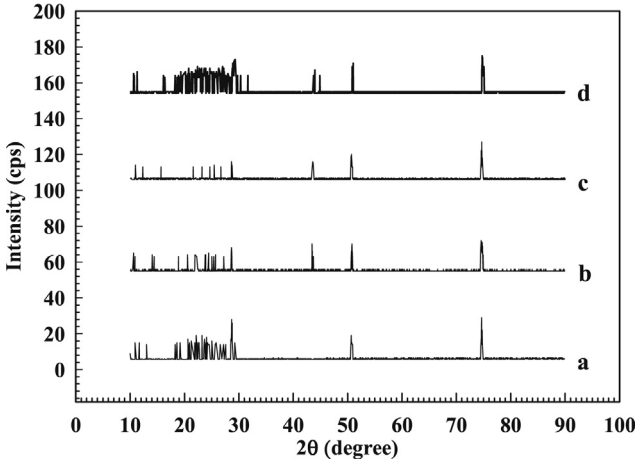

Fig. 7 – XRD results obtained from gel@LiMo catalysts prepared with calcined MoO_3 for 0 h (a), 5 h (b), 8 h (c), 15 h (d) at 500 °C.

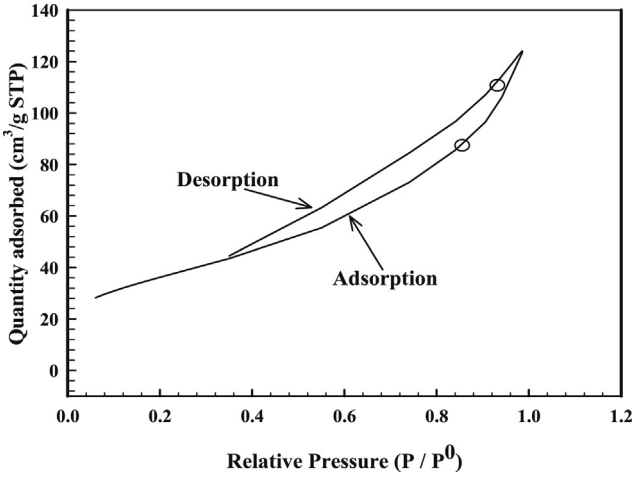

Fig. 8 – Nitrogen adsorption–desorption isotherms of gel@LiMo catalysts.

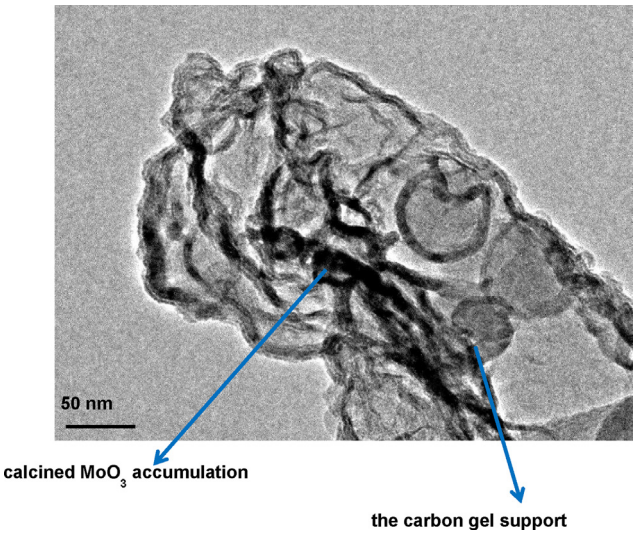

Fig. 9 – TEM images of gel@LiMo catalysts in 50 nm.

$$Li \leftrightharpoons Li^{+} + e^{-}$$

$$Li^{+} + e^{-} + O_2 \leftrightharpoons LiO_2$$

$$Li^{+} + e^{-} + LiO_2 \leftrightharpoons Li_2O_2$$

forward direction and backward direction indicate discharge and charge processes, respectively.

Conclusions

A macroporous gel@LiMo catalyst was prepared by sol–gel method and its performance was studied in oxygen reduction and evolution reaction in the lithium air battery. The prepared catalyst was tested with cyclic voltammetry, electrochemical impedance spectroscopy cathodic polarization curves and discharge–charge curves. The best combination and calcination time were determined with cyclic voltammetry. The gel@LiMo catalyst exhibited the best electrocatalytic activity and electrochemical performance at 8 h calcinated MoO_3. The overpotential behavior was analyzed using cathodic polarization curves. The gel@LiMo catalyst has the highest current density at the lowest overpotential as well as the lowest polarization resistance at a specific overpotential compared with the other catalysts. In the SEM and TEM images it is seen that at 8 h the surface structure of the gel@LiMo catalyst had been transformed into a shaped morphology which has wide and large surface area. A phase transformation from a hexagonal phase to a more stable orthorhombic MoO_3 (α-MoO_3) phase was observed in the XRD pattern of the gel@LiMo samples at 8 h. The N_2 adsorption and desorption isotherms were taken to calculate the surface area, pore volume and pore size. It was determined by BET method that gel@LiMo catalyst had a macroporous structure. The porous structure improved the catalytic efficiency. These results prove that the gel@LiMo catalyst showed good electrocatalytic efficiency at oxygen reduction and evolution reactions. It suggested that the prepared gel@LiMo can be used as a cathode catalyst for the lithium-air battery.

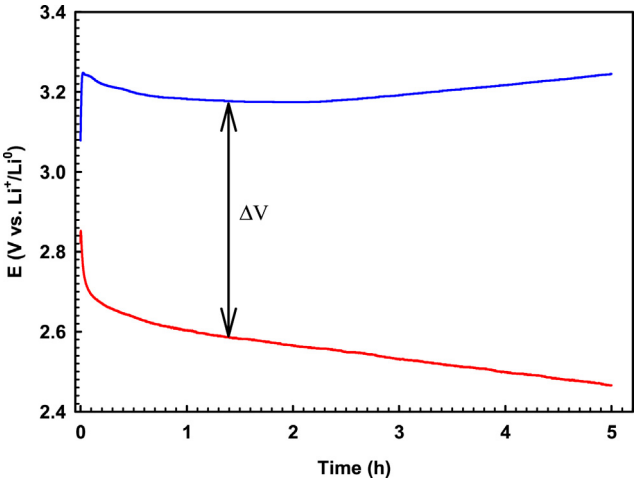

Fig. 10 – OER and ORR curves of gel@LiMo catalyst at a current density of 0.05 mA cm^{-2}.

Acknowledgments

The authors are greatly thankful to The Scientific and Technological Research Council of Turkey (TUBITAK) with project number 112T532 for financial support.

REFERENCES

[1] Wang H, Xie K, Wang L, Han Y. N-methyl-2-pyrrolidone as a solvent for the non-aqueous electrolyte of rechargeable Li-air batteries. J Power Sources 2012;219:263–71.
[2] Ida S, Thapa AK, Hidaka Y, Okamoto Y, Matsuka M, Hagiwara H, et al. Manganese oxide with a card-house-like structure reassembled from nanosheets for rechargeable Li-air battery. J Power Sources 2012;203:159–64.
[3] Cecchetto L, Salomon M, Scrosati B, Croce F. Study of a Li–air battery having an electrolyte solution formed by a mixture of an ether-based aprotic solvent and an ionic liquid. J Power Sources 2012;213:233–8.
[4] Abraham K, Jiang Z. A polymer electrolyte-based rechargeable lithium/oxygen battery. J Electrochem Soc 1996;143:1–5.
[5] Zu C-X, Li H. Thermodynamic analysis on energy densities of batteries. Energy Environ Sci 2011;4:2614–24.
[6] Ma Z, Yuan X, Sha H-D, Ma Z-F, Li Q. Influence of cathode process on the performance of lithium-air batteries. Int J Hydrogen Energy 2013;38:11004–10.
[7] Girishkumar G, McCloskey B, Luntz A, Swanson S, Wilcke W. Lithium– air battery: promise and challenges. J Phys Chem Lett 2010;1:2193–203.
[8] Yang C-C. Preparation and characterization of electrochemical properties of air cathode electrode. Int J Hydrogen Energy 2004;29:135–43.
[9] Beattie S, Manolescu D, Blair S. High-capacity lithium–air cathodes. J Electrochem Soc 2009;156:A44–7.
[10] Cui Y, Wen Z, Liu Y. A free-standing-type design for cathodes of rechargeable Li–O_2 batteries. Energy & Environ Sci 2011;4:4727–34.

[11] Andrei P, Zheng JP, Hendrickson M, Plichta E. Some possible approaches for improving the energy density of Li-air batteries. J Electrochem Soc 2010;157:A1287–95.

[12] Crowther O, Meyer B, Morgan M, Salomon M. Primary Li-air cell development. J Power Sources 2011;196:1498–502.

[13] Zhang G, Zheng J, Liang R, Zhang C, Wang B, Au M, et al. α-MnO_2/carbon nanotube/carbon nanofiber composite catalytic air electrodes for rechargeable lithium-air batteries. J Electrochem Soc 2011;158:A822–7.

[14] Gao Y, Wang C, Pu W, Liu Z, Deng C, Zhang P, et al. Preparation of high-capacity air electrode for lithium-air batteries. Int J Hydrogen Energy 2012;37:12725–30.

[15] Wang H, Yin F, Li G, Chen B, Wang Z. Preparation, characterization and bifunctional catalytic properties of MOF(Fe/Co) catalyst for oxygen reduction/evolution reactions in alkaline electrolyte. Int J Hydrogen Energy 2014;39:16179–86.

[16] Yavuz E, Özdokur KV, Çakar İ, Koçak S, Ertaş FN. Electrochemical preparation, characterization of molybdenum-oxide/platinum binary catalysts and its application to oxygen reduction reaction in weakly acidic medium. Electrochim Acta 2015;151:72–80.

[17] Wang L, Yin F, Yao C. N-doped graphene as a bifunctional electrocatalyst for oxygen reduction and oxygen evolution reactions in an alkaline electrolyte. Int J Hydrogen Energy 2014;39:15913–9.

[18] Débart A, Paterson AJ, Bao J, Bruce PG. α-MnO_2 nanowires: a catalyst for the O_2 electrode in rechargeable lithium batteries. Angew Chem 2008;120:4597–600.

[19] Débart A, Bao J, Armstrong G, Bruce PG. An O_2 cathode for rechargeable lithium batteries: the effect of a catalyst. J Power Sources 2007;174:1177–82.

[20] Thapa AK, Saimen K, Ishihara T. Pd/MnO_2 air electrode catalyst for rechargeable lithium/air battery. Electrochem Solid-State Lett 2010;13:A165–7.

[21] Thapa AK, Ishihara T. Mesoporous α-MnO_2/Pd catalyst air electrode for rechargeable lithium–air battery. J Power Sources 2011;196:7016–20.

[22] Lu Y-C, Xu Z, Gasteiger HA, Chen S, Hamad-Schifferli K, Shao-Horn Y. Platinum– gold nanoparticles: a highly active bifunctional electrocatalyst for rechargeable lithium– air batteries. J Am Chem Soc 2010;132:12170–1.

[23] Sakamoto K, Hirayama M, Konishi H, Sonoyama N, Dupré N, Guyomard D, et al. Structural changes in surface and bulk $LiNi_0.5Mn_0.5O_2$ during electrochemical reaction on epitaxial thin-film electrodes characterized by in situ X-ray scattering. PCCP 2010;12:3815–23.

[24] Wang Y, Cao G. Developments in nanostructured cathode materials for high-performance lithium-ion batteries. Adv Mater 2008;20:2251–69.

[25] Drezen T, Kwon N-H, Bowen P, Teerlinck I, Isono M, Exnar I. Effect of particle size on $LiMnPO_4$ cathodes. J Power Sources 2007;174:949–53.

[26] Zhao T, Li L, Chen S, Chen R, Zhang X, Lu J, et al. The effect of chromium substitution on improving electrochemical performance of low-cost Fe–Mn based Li-rich layered oxide as cathode material for lithium-ion batteries. J Power Sources 2014;245:898–907.

[27] Mohan P, Paruthimal Kalaignan G. Structure and electrochemical performance of surface modified $LaPO_4$ coated $LiMn_2O_4$ cathode materials for rechargeable lithium batteries. Ceram Int 2014;40:1415–21.

[28] Wachs IE. Recent conceptual advances in the catalysis science of mixed metal oxide catalytic materials. Catal Today 2005;100:79–94.

[29] Yang J, Xu JJ. Nanoporous amorphous manganese oxide as electrocatalyst for oxygen reduction in alkaline solutions. Electrochem Commun 2003;5:306–11.

[30] Esmaili P, Dincer I, Naterer GF. Energy and exergy analyses of electrolytic hydrogen production with molybdenum-oxo catalysts. Int J Hydrogen Energy 2012;37:7365–72.

[31] Yan Z, Xie J, Jing J, Zhang M, Wei W, Yin S. MoO_2 nanocrystals down to 5 nm as Pt electrocatalyst promoter for stable oxygen reduction reaction. Int J Hydrogen Energy 2012;37:15948–55.

[32] Farsak M, Telli E, Tezcan F, Akgül FS, Yüce AO, Kardaş G. The electrocatalytic properties of lithium copper composite in the oxygen reduction reaction. Electrochim Acta 2014;148:276–82.

[33] Song M-K, Park S, Alamgir FM, Cho J, Liu M. Nanostructured electrodes for lithium-ion and lithium-air batteries: the latest developments, challenges, and perspectives. Mater Sci Eng R: Reports 2011;72:203–52.

[34] Chithambararaj A, Bose AC. Investigation on structural, thermal, optical and sensing properties of meta-stable hexagonal MoO_3 nanocrystals of one dimensional structure. Beilstein J Nanotechnol 2011;2:585–92.

[35] Ohkuma H, Uechi I, Imanishi N, Hirano A, Takeda Y, Yamamoto O. Carbon electrode with perovskite-oxide catalyst for aqueous electrolyte lithium-air secondary batteries. J Power Sources 2013;223:319–24.

[36] Kichambare P, Kumar J, Rodrigues S, Kumar B. Electrochemical performance of highly mesoporous nitrogen doped carbon cathode in lithium–oxygen batteries. J Power Sources 2011;196:3310–6.

[37] Hu S-K, Cheng G-H, Cheng M-Y, Hwang B-J, Santhanam R. Cycle life improvement of ZrO_2-coated spherical LiNi1/3Co1/3Mn1/3O2 cathode material for lithium ion batteries. J Power Sources 2009;188:564–9.

[38] Solmaz R, Kardaş G, Yazıcı B, Erbil M. Adsorption and corrosion inhibitive properties of 2-amino-5-mercapto-1, 3, 4-thiadiazole on mild steel in hydrochloric acid media. Colloids Surf A: Physicochem Eng Asp 2008;312:7–17.

[39] Solmaz R, Kardaş G, Culha M, Yazıcı B, Erbil M. Investigation of adsorption and inhibitive effect of 2-mercaptothiazoline on corrosion of mild steel in hydrochloric acid media. Electrochim Acta 2008;53:5941–52.

[40] Wu Y, Ming J, Zhuo L, Yu Y, Zhao F. Simultaneous surface coating and chemical activation of the Li-rich solid solution lithium rechargeable cathode and its improved performance. Electrochim Acta 2013;113:54–62.

[41] Wang Q, Liu J, Murugan AV, Manthiram A. High capacity double-layer surface modified Li $[Li_{0.2}Mn_{0.54}Ni_{0.13}Co_{0.13}]O_2$ cathode with improved rate capability. J Mater Chem 2009;19:4965–72.

[42] Wang J, Qiu B, Cao H, Xia Y, Liu Z. Electrochemical properties of 0.6 Li $[Li_{1/3}Mn_{2/3}]O_2$ −0.4$LiNi_xMn_yCo_{1-x-y}O_2$ cathode materials for lithium-ion batteries. J Power Sources 2012;218:128–33.

[43] Nassar MY, Attia AS, Alfallous KA, El-Shahat M. Synthesis of two novel dinuclear molybdenum (0) complexes of quinoxaline-2, 3-dione: new precursors for preparation of α-MoO_3 nanoplates. Inorg Chim Acta 2013;405:362–7.

[44] Donohue M, Aranovich G. Classification of Gibbs adsorption isotherms. Adv Colloid Interface Sci 1998;76:137–52.

[45] Lu J, Amine K. Recent research progress on non-aqueous lithium-air batteries from Argonne National Laboratory. Energies 2013;6:6016–44.

[46] Yang W, Salim J, Li S, Sun C, Chen L, Goodenough JB, et al. Perovskite Sr 0.95 Ce 0.05 CoO 3– δ loaded with copper nanoparticles as a bifunctional catalyst for lithium-air batteries. J Mater Chem 2012;22:18902–7.

[47] Yang W, Salim J, Ma C, Ma Z, Sun C, Li J, et al. Flowerlike Co_3O_4 microspheres loaded with copper nanoparticle as an efficient bifunctional catalyst for lithium–air batteries. Electrochem Commun 2013;28:13–6.